Drift time estimation by dynamic time warping

Tianci Cui and Gary F. Margrave
CREWES, University of Calgary
cuit@ucalgary.ca

Summary

The drift time is the difference in traveltime at the seismic frequency and the sonic logging frequency in anelastic media. The stationary synthetic seismogram needs drift time correction to tie the nonstationary seismic trace. Without knowledge of Q or a check-shot survey, dynamic time warping can estimate the drift time associated with apparent Q automatically by matching the stationary and nonstationary seismograms. After applying drift time correction to the stationary seismogram, the residual constant-phase between it and the nonstationary seismogram is small and almost constant with traveltime. The final crosscorrelation coefficient of stationary and nonstationary seismograms can be as high as 0.95.

Drift time

A density log (black) and a p-wave velocity log (blue) measured from Hussar well 12-27 are plotted in Figure 1. According to the constant-Q theory (Kjartansson, 1979), velocity is dependent on frequency by

$$v(f_s) = v(f_w)\left[1 - \frac{1}{\pi Q} ln\left(\frac{f_s}{f_w}\right)\right]^{-1} \tag{1}$$

where f_w is the well logging frequency and f_s is the seismic frequency. A fake Q log (green) is constructed from assumed linear relationships between Q and the density and p-wave velocity logs. Assume $f_w = 12.5\ kHz$ and $f_s = 30\ Hz$, the p-wave velocity experienced by seismic waves is calculated using equation 1 and plotted in red, which is systematically slower than that measured by the sonic tool. Convert the depth to two-way vertical traveltime at f_w and f_s respectively, and their difference is the theoretical drift time $drift(t)$ (Figure 2).
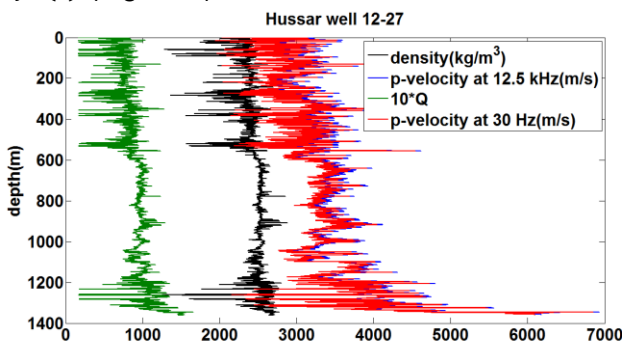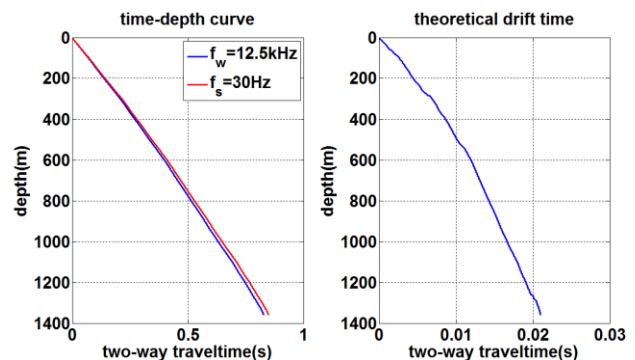

FIG 1: Logs from Hussar well 12-27.

FIG 2: Time-depth curves (left) and the theoretical drift time (right).

In Figure 3, the reflectivity is calculated from the density and p-wave velocity logs. Convolving the reflectivity with a minimum-phase wavelet whose dominant frequency is $30\ Hz$, a stationary seismogram $s(t)$ is constructed to simulate the synthetic seismogram. To include Q effects in the seismogram, a synthetic zero-offset VSP model is constructed using the reflectivity, the fake Q log and the wavelet based on the algorithm described by Ganley (1981). Figure 4 shows the primary-only upgoing wavefield, where the leftmost trace, namely the trace recorded by the surface receiver, is the nonstationary seismogram

$s_q(t)$ with Q effects to simulate the recorded seismic trace, which is plotted in red in Figure 5 top panel. In comparison to $s(t)$ (blue), $s_q(t)$ shows progressive attenuation effects, such as diminishing amplitude, widening wavelets and delaying events, among which the delay is caused by the drift time. The maximum crosscorrelation coefficient between $s(t)$ and $s_q(t)$ is about 0.41 at a lag of -5 (a negative lag indicates $s_q(t)$ is delayed relative to $s(t)$).

In the procedure of seismic-to-well ties, the synthetic seismogram $s(t)$ is to be matched with the recorded seismic trace $s_q(t)$. In Figure 5 bottom panel, $s(t)$ is first corrected to the traveltime at the seismic frequency using the theoretical drift time $drift(t)$

$$s_{corr}(t) = s\big(t + drift(t)\big), \tag{2}$$

where $s_{corr}(t)$ is the stationary seismogram after drift time correction, and it reaches a correlation of over 0.90 with $s_q(t)$. Then, the residual constant-phase between $s_{corr}(t)$ and $s_q(t)$ is measured in a sliding Gaussian window of $0.1\ s$ width and $0.01\ s$ increment. As is shown in Figure 6 top panel, the residual phase is small and almost constant along traveltime. Finally, a time-variant amplitude balancing and a time-variant constant-phase rotation are done on $s_q(t)$ relative to $s_{corr}(t)$ in the same sliding Gaussian window. The final matching of $s(t)$ and $s_q(t)$ is about 0.94 at a lag of -0.1 (Figure 6 bottom panel).
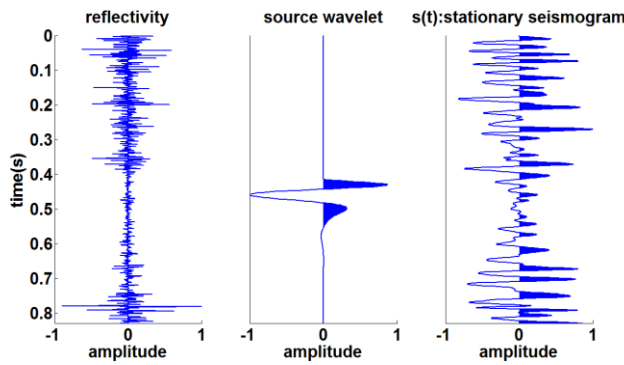

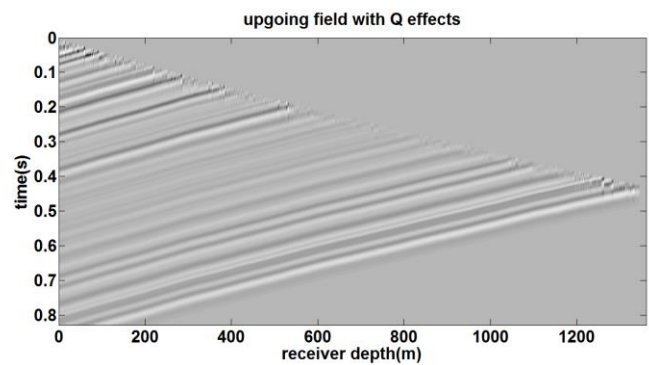FIG 3: Construction of the stationary seismogram.

FIG 4: The primary-only upgoing field with Q effects. The leftmost trace is the nonstationary seismogram.
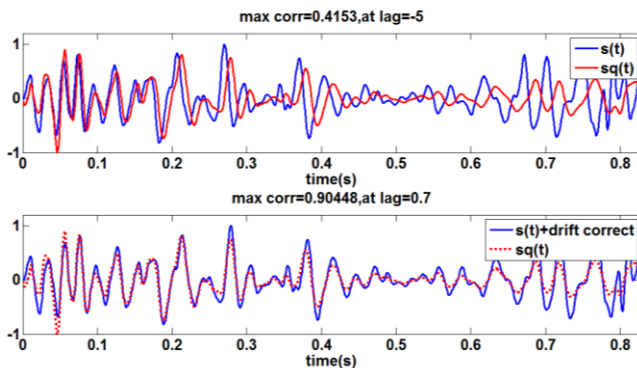

FIG 5: Stationary and nonstationary seismograms (top). Drift time correction on stationary seismogram (bottom).
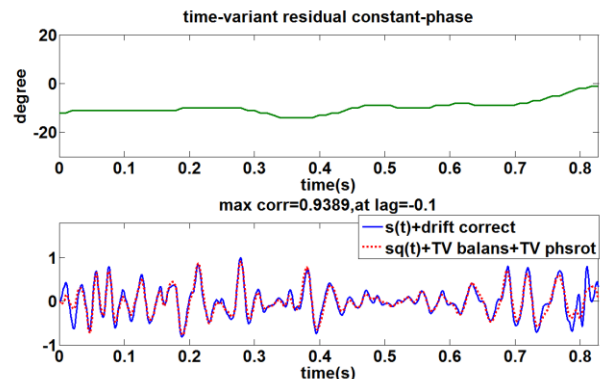

FIG 6: Time-variant residual constant-phase between $s_{corr}(t)$ and $s_q(t)$ (top). Final matching of $s(t)$ and $s_q(t)$ (bottom).

Dynamic time warping

In seismic-to-well ties, drift time correction is necessary to match the stationary synthetic seismogram to the nonstationary seismic trace. In industrial practice, calculation of drift time needs knowledge of Q, or a check-shot survey or manually stretching and squeezing the synthetic seismogram. Without this information, dynamic time warping (DTW) is able to estimate the drift time automatically by matching the stationary seismogram and the nonstationary seismogram caused by anelastic attenuation. Dynamic

time warping is based on constrained optimization algorithm and is realized by dynamic programming. It is more sensitive to the rapid-varying time shift than time-variant crosscorrelation (Hale, 2012).

In dynamic time warping, the stationary and nonstationary seismograms are expressed in terms of sample number n, namely, $s(n)$ and $s_q(n)$. To estimate the drift time between the two seismograms, the alignment error array $e(m, n)$ is calculated according to

$$e(m,n) = \left[s\left(n \right) - s_q \left(n + m \right) \right]^2, n = 1, 2, \ldots, N \qquad (3)$$

where lag m is set to be $-L \leq m \leq L$. Namely, for each sample number n, we calculate the squared differences between $s\left(n \right)$ and the most adjacent $2L + 1$ samples to $s_q\left(n \right)$. The alignment error array, computed for the two seismograms in Figure 5 top panel with $N = 829$ and $L = 50$, is shown in Figure 7, where a darker color indicates a larger alignment error. Representing the continuous theoretical drift time as discrete theoretical drift lag and plotting it in red on top of the alignment error array in Figure 8, we can observe that the alignment error is nearly zero along the theoretical drift lag. There are 101^{829} paths traveling from $n = 1$ to 829, among which the drift lag sequence is the one whose cumulative error summing along its path is the minimum. However, searching 101^{829} paths is far beyond the computation ability of a modern computer. Applying suitable constraints to this problem can make it solvable by DTW.

DTW computes a sequence $u(n) = [u(1), u(2), \ldots, u(N)]$ that approximates the theoretical drift lag sequence by solving the following optimization problem:

$$u(1:N) = \underset{m(1:N)}{\arg\min} D[m(1:N)], \qquad (4)$$

where

$$D[m(1:N)] = \sum_{n=1}^{N} e\big(n, m(n)\big) \qquad (5)$$

subject to the constraint

$$\sum_{k=1}^{b} |m(n - k + 1) - m(n - k)| \leq 1 \qquad (6)$$

Equation 6 indicates that the possible drift lag sequence $m(1:N)$ searched by DTW is constrained to change in blocks of b samples. That is reasonable for the drift time in the real world, which does not vary rapidly from one sample to the next. Figure 9 shows the estimated drift time by DTW when $b = 1$ (top panel) and $b = 10$ (bottom panel), and the latter is smoother and more approximate to the theoretical drift time due to a further constraint. The estimated drift time is then used to correct the stationary seismogram $s(t)$, followed by a time-variant amplitude balancing and a time-variant constant-phase rotation on $s_q(t)$ as shown in Figure 10. The final matching of $s(t)$ and $s_q(t)$ is about 0.95 at a lag of 0.2.
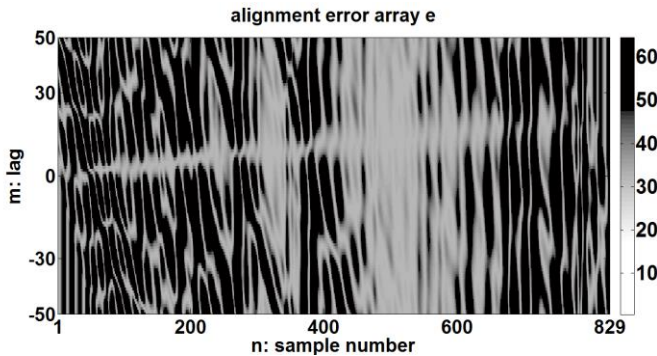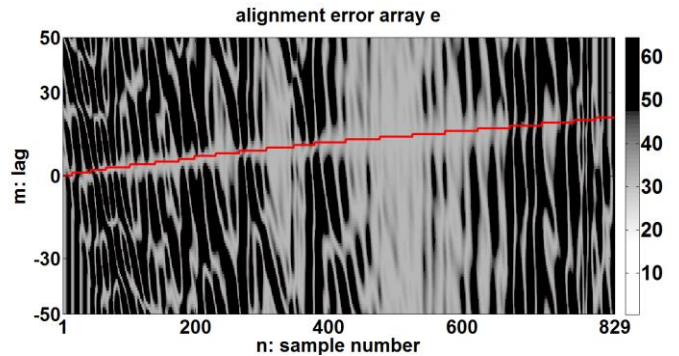

FIG 7: The alignment error array.

FIG 8: The alignment error array (background) and the theoretical drift lag sequence (red curve).
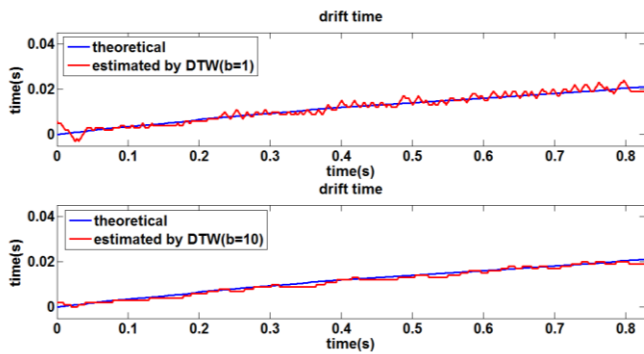
FIG 9: Estimated drift time when $b = 1$ (top) and $b = 10$ (bottom) in comparison with the theoretical drift time.
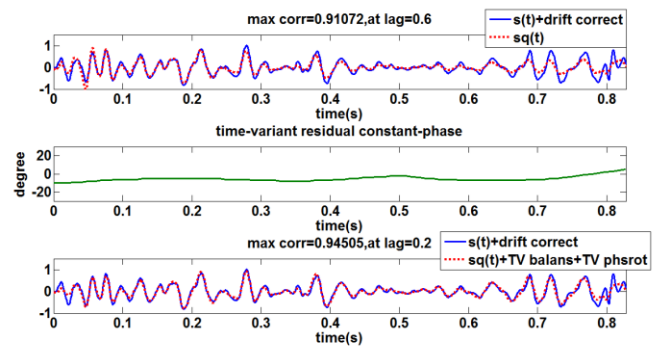

FIG 10: Drift time correction on $s(t)$ using the estimated drift time (top). The time-variant residual constant-phase (middle). Final matching (bottom).

Inclusion of internal multiples

A more realistic 1D seismogram containing internal multiples is constructed using the VSP algorithm based on the same well logs, Q and wavelet. Figure 11 shows the upgoing wavefield of the synthetic zero offset VSP with both Q and internal multiple effects. The leftmost trace is the nonstationary seismogram $s_{qi}(t)$ with both Q and internal multiple effects, which is plotted in black in Figure 12 top panel compared to the stationary seismogram $s(t)$ (blue) and the nonstationary seismogram $s_q(t)$ (red) with Q effects only. We can observe that $s_{qi}(t)$ appears more attenuation than $s_q(t)$. The drift time of the two nonstationary seismograms with respect to the stationary one is estimated by DTW using $b = 10$ shown in Figure 12 bottom panel. As first discussed by O'Doherty and Anstey (1971), short-path multiples cause stratigraphic filtering effects that are indistinguishable from anelastic attenuation, which leads to an apparent Q whose value is lower than the intrinsic Q. Thus, the drift time estimated from $s_{qi}(t)$ is systematically higher than the theoretical one calculated from the fake Q log and their difference becomes larger at longer traveltime when more internal multiples are produced.
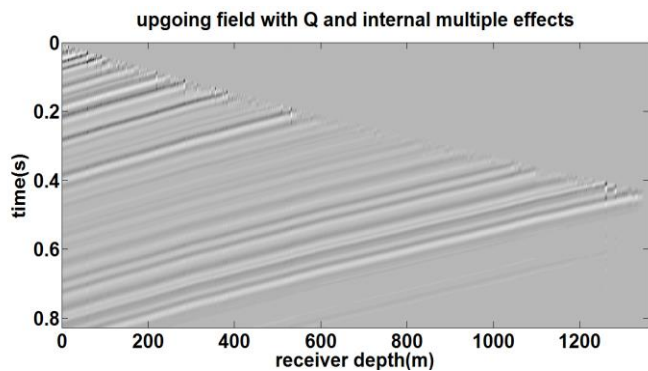

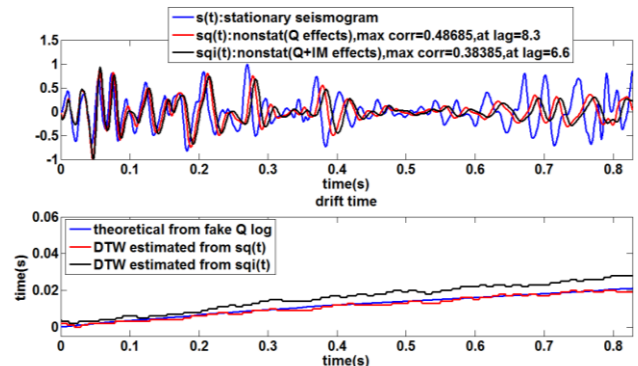FIG 11: Upgoing wavefield with both Q and internal multiple effects.

FIG 12: Stationary and nonstationary seismograms (top). Theoretical and estimated drift time (bottom).

Conclusions

Dynamic time warping succeeds in estimating drift time automatically without knowledge of Q or a check-shot survey. Application of drift time correction results in a much simpler residual phase. DTW estimates drift time associated with apparent Q including both intrinsic and stratigraphic effects.

Acknowledgements

References

Ganley, D. C., 1981, A method for calculating synthetic seismograms which include the effects of absorption and dispersion, Geophysics, Aug 1981, Vol. 46, No. 8, pp. 1100-1107.

Hale, D., 2013, Dynamic warping of seismic images: Geophysics, 78(2), S105-S115.

Kjartansson, E, 1979, Constant Q-wave Propagation and Attenuation, Journal of Geophysical Research, 84, 4737-4748.

O'Doherty, R. F., and Anstey, N. A., 1971, Reflections on amplitudes, Geophysical Prospecting, 19, 430-458.